Journal of Hydrology 551 (2017) 746–755

Contents lists available at ScienceDirect

Journal of Hydrology

journal homepage: www.elsevier.com/locate/jhydrol

Research papers

Resistivity imaging reveals complex pattern of saltwater intrusion along Monterey coast

Meredith Goebel [a,*], Adam Pidlisecky [b,c], Rosemary Knight [a]

[a] Stanford University, United States
[b] ARANZ Geo, New Zealand
[c] University of Calgary, Canada

ARTICLE INFO

Article history:
Available online 22 February 2017

Keywords:
Electrical Resistivity Tomography (ERT)
Saltwater intrusion
Monterey
Coastal aquifer
Groundwater management

ABSTRACT

Electrical Resistivity Tomography data were acquired along 40 km of the Monterey Bay coast in central California. These data resulted in electrical resistivity images to depths of approximately 280 m.b.s.l., which were used to understand the distribution of freshwater and saltwater in the subsurface, and factors controlling this distribution. The resulting resistivity sections were interpreted in conjunction with existing data sets, including well logs, seismic reflection data, geologic reports, hydrologic reports, and land use maps from the region. Interpretation of these data shows a complex pattern of saltwater intrusion resulting from geology, pumping, and recharge. The resistivity profiles were used to identify geological flow conduits and barriers such as palaeo-channels and faults, localized saltwater intrusion from individual pumping wells, infiltration zones of surface fresh and brackish water, and regions showing improvements in water quality due to management actions. The use of ERT data for characterizing the subsurface in this region has led to an understanding of the spatial distribution of freshwater and saltwater at a level of detail unattainable with the previously deployed traditional well based salinity mapping and monitoring techniques alone. Significant spatial variability in the extent and geometry of intrusion observed in the acquired data highlights the importance of adopting continuous subsurface characterization methods such as this one.

1. Introduction

A coastal region represents a dynamic zone where fresh groundwater in the coastal aquifers interacts with saline ocean water. The location of the freshwater-saltwater interface is governed by the density and pressure differences on the two sides of the interface and the subsurface hydrologic properties that control fluid movement. Saltwater intrusion is the process in which this interface moves landward, with saltwater then occupying parts of the aquifer that were once fresh. While this process has been observed and documented throughout the world for over a century (Bear et al., 1999), climate change, growing water demands, and manipulation of natural hydrologic systems have led to saltwater intrusion being considered a significant threat to future freshwater resources globally (Kinzelbach et al., 2003; Barlow and Reichard, 2009; Werner et al., 2013).

Saltwater intrusion can have a number of significant economic and environmental impacts, including diminished freshwater storage capacity, contamination of freshwater production wells, soil salinization, and decreased nutrient laden freshwater discharge to marine ecosystems (Johannes, 1980; Taniguchi et al., 2002; Werner et al., 2013). A number of steps can be taken to attempt to slow the rate of saltwater intrusion, including spatial and temporal changes in the extent of groundwater pumping, in land-use, in surface water diversions, and in artificial recharge (Abarca et al., 2006). What is needed however is a way to prioritize these actions, or combinations of actions, so as to optimize the impact on saltwater intrusion. This requires an accurate understanding of the current distribution of freshwater and saltwater, that can be used to predict future locations in response to these, and other, actions (Sanford and Pope, 2009).

Saltwater intrusion is traditionally mapped and monitored using measurements made in wells and predictive flow models (Werner et al., 2013). There are a number of limitations with these methods. Measurements made in wells provide point data, which may fail to capture the spatial complexity in subsurface conditions. Improving spatial coverage with additional wells can be cost

* Corresponding author at: 397 Panama Mall, 3rd Floor, Stanford, CA 94305-2215, United States.
E-mail address: mgoebel@stanford.edu (M. Goebel).

http://dx.doi.org/10.1016/j.jhydrol.2017.02.037
0022-1694/

prohibitive (Ogilvy et al., 2009). Additionally, salinity measurements from wells can be flux-averaged concentrations, and head measurements in wells are affected by the density of the water column so can be misinterpreted in the presence of unknown salt water, and are susceptible to measurement, instrument, and time lag errors (Carrera et al., 2009; Post and Von Asmuth, 2013). Models are generally calibrated by matching historic head values in wells and/or matching salinity values from well samples (Carrera et al., 2009), thus all the limitations of well data are carried over into the model calibration. Given these limitations there is significant opportunity for additional methods of mapping and monitoring the distribution of saltwater in the subsurface for improved management of coastal aquifers.

Geophysical methods are often used to complement well data, improving the understanding of spatial heterogeneity away from the wells. Electrical geophysical methods are particularly well suited to characterizing saltwater-intruded regions, as they are sensitive to changes in subsurface conductivity which are often caused by changes in pore fluid salinity (Knight and Endres, 2005; Goldman and Kafri, 2006). One such electrical method, Electrical Resistivity Tomography (ERT) has been demonstrated in a number of studies in recent years to be useful for this application. Martínez et al. (2009) found ERT to be useful in identifying zones of intrusion in a Spanish coastal aquifer, with excellent agreement between ERT profiles and borehole measurements. This study produced resistivity profiles up to 555 m long, imaging down to 106 m. De Franco et al. (2009) demonstrated the effectiveness of time-lapse ERT to monitor the dynamics of saltwater intrusion in response to environmental changes in Venice, Italy, imaging to depths of up to 60 m with profiles 300 m long. Additionally, studies by Maillet et al. (2005), Batayneh (2006), Rey et al. (2013), Zarroca et al. (2011) and Pidlisecky et al. (2015), and others have illustrated the ability of ERT to locate and define the geometries of saltwater bodies in groundwater aquifers, and show an increasing use of this method in saltwater intrusion investigations. While these studies have highlighted the utility of ERT for these environments, their use of ERT have been limited in spatial extent, thus precluding a comprehensive study of the controls on the location and extent of saltwater intrusion at the basin or larger. In larger basins with complex or variable geology, small-scale imaging makes exploration and interpretation difficult as only a small portion of the relevant area is illuminated.

Few groundwater ERT studies have been conducted at the basin scale (multiple kilometers), commonly needed to make regional management decisions. In the past decade, the mineral and petroleum industries have addressed the challenges of acquiring data at this scale (1–30+ km), with many accompanying developments in acquisition methods (Bauman, 2005; Loke et al., 2013). These developments, which include rapid data collection with multichannel systems, large distances between electrodes, and an acquisition approach that increases data coverage, can achieve unprecedented depths of high resolution imaging with ERT (Baines et al., 2002; Loke, 1999; Pidlisecky et al., 2015). Long-offset ERT now has the potential to provide insight, with short turn-around time, into aquifer lithology and fluid distribution for costs comparable to those of monitoring well programs.

This study took place along the coast of the Monterey Bay in central California, where multiple over-drafted basins have experienced, or are threatened by, saltwater intrusion. A pilot study (Pidlisecky et al., 2015) conducted along the southern end of the Monterey Bay coast tested the long-offset ERT method on a 7 km stretch, with the goals of: (1) demonstrating the viability of using long-offset ERT to image the distribution of subsurface freshwater and saltwater over a large spatial extent, and (2) gaining insight into the distribution and geologic controls of seawater intrusion in the Monterey Bay region. This pilot study was able to determine electrical resistivity values to a depth of 150 m, and gave significant insight into the spatial distribution of saltwater intrusion, and role of the local geology in controlling intrusion along the transect. The success of this pilot study motivated us to further pursue these goals by acquiring long offset ERT data along a 40 km stretch of coast, imaging to a depth of ~280 m; to our knowledge the most extensive high-resolution image ever obtained for imaging saltwater intrusion at the basin scale. This new study, presented here, reveals the complex nature of saltwater intrusion in the Monterey Bay region, and highlights ways in which ERT can provide key information about the controls on saltwater intrusion and can be used to identify the necessary scale of management, and support decision-making. This demonstration of the utility of ERT for exploratory imaging at this specific site will hopefully be used as a guide for others to apply this method to similarly impacted coastal basins around the world.

2. Study area

This location of the study is shown in the maps in Fig. 1. Along Monterey Bay coast, intensively farmed land meets a national marine sanctuary. With limited surface water resources, pumping from coastal aquifers provides >80% of the freshwater in this region, with that percentage reaching 99% in Monterey County (California Water Foundation, 2014). Extensive pumping has lead to significant saltwater intrusion in the region, which was noted as early as the 1930's (Yates et al., 2005), and to date has extended up to 16 km inland in the Salinas River Valley, as shown in Fig. 1b (Monterey County Water Resources Agency, 2014). Addressing the issue of saltwater intrusion in this region requires balancing the needs of a multi-billion dollar agricultural industry, domestic and industrial users, and the environment, across many governmental management agencies (California Water Foundation, 2014; Monterey County Agricultural Commissioner, 2015).

Fig. 1a shows the location of ERT data acquisition along the coast of Monterey Bay, drawn in black, as well as the boundaries of the groundwater basins in the region (Department of Water Resources, 2003). Fig. 1b shows the location of key information used in the interpretation of the ERT data. In red are the numerous faults found throughout this region (U.S. Geological Survey and California Geological Survey, 2006). Important to note is the regional pattern of northwest/southeast trending faults, which intersect the ERT transect in the south but not in the north. In blue are significant rivers. Also shown are geologic cross-sections (Brabb et al., 1997; Feeney, 2007; Hanson et al., 2002; RBF, 2014) that are compared to the ERT resistivity data in the results and discussion section. Shown in orange are coastal wells with induction logs, which are also compared to the ERT resistivity data in the results and discussion section. Shown in gray is the currently mapped extent of saltwater intrusion, based on well water sampling (Pajaro Valley Water Management District, 2016; Monterey County Water Resources Agency, 2014). Within the Salinas Valley, extent of intrusion is separately reported for the upper and lower aquifer units. These two boundaries different are shown, with the more inland boundary belonging to the upper aquifers. Important to note however, is that these maps only show the extent of intrusion as reported by local agencies as interpolated spatial information, intrusion is known to extend further to the North, but is not reported in a way that can be included in these maps.

It would have been extremely helpful to have pumping data from the area to inform our interpretations. Unfortunately, records of groundwater pumping are not legally required by the state of California at this time. Therefore, information about pumping is inconsistent across the study area, and often only anecdotally available from water managers who enter into confidentiality

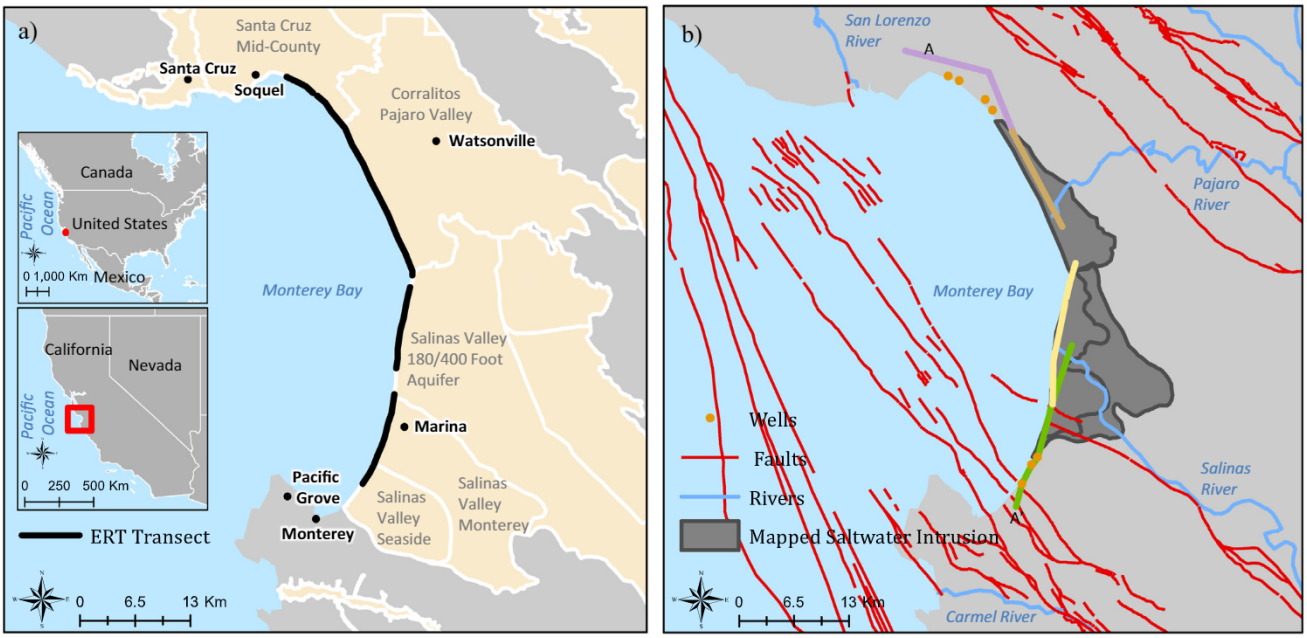

Fig. 1. a) Map of field site along the coast of Monterey Bay showing the locations of the ERT transects (in black) and groundwater basin boundaries taken from Department of Water Resources (2003). b) Map of the field site with the locations of key information used in the ERT interpretation, including wells with induction logs in orange, geologic cross-sections from Brabb et al. (1997), Hanson et al. (2002), RBF (2014) and Feeney (2007) (in purple, brown, yellow, and green respectively), faults in red, rivers in blue, and the current mapped extent of saltwater intrusion in gray. End points of the coastal conceptual cross-section in Fig. 2 are labeled A and A′.

agreements with private well owners who voluntarily record and pass on this information. Furthermore, while well drilling reports are required to be submitted to the state, these are in hard copy format and not readily available to the public nor are they standardized in terms of interpretation and content.

Our study area spans three groundwater basins: The Santa Cruz Mid-County, Pajaro Valley (a Subbasin of the Corralitos Basin), and Salinas Valley, which is further subdivided into the 180-Foot/400-Foot and Seaside Subbasin as shown in Fig. 1a. A conceptual cross-section of the formations within these basins along the Monterey Bay coast is shown in Fig. 2. The endpoints of the cross-section (A and A′) are shown in Fig. 1b. The dashed box outlines the region spanned by the inverted ERT resistivity profiles. The conceptual cross-section was developed through compilation of cross-sections from Brabb et al. (1997), Hanson et al. (2002), WRIME (2003), Yates et al. (2005) and Feeney (2007). The primary stratigraphic units in this region, from deepest to shallowest, are the Granitic Basement (Kgr); an unnamed sandstone (Tus); the Monterey Formation (Tm), a marine shale and mudstone unit, considered the base of the water bearing units; the Santa Margarita Formation (Tsm), a poorly consolidated marine sandstone and an important freshwater unit; the Purisima Formation (Tp), a poorly consolidated marine deposit of sandstone, siltstone, and mudstone, and a minor water bearing unit; the Paso Robles Formation (QTp, often combined with the Purisima Formation), consisting of beds of lenticular sand, gravel, silt, and clay, and an important water bearing unit; the Aromas Sand Formation (Qar), a unit consisting of cross-bedded sands and some clays, and an important water bearing unit; and Surficial deposits (Qal). OSR ('other sedimentary regions') on the conceptual cross section includes the Santa Margarita Formation and Monterey Formation. The thickness and extent of each of these units varies significantly across the study area (Department of Water Resources, 2003; Monterey County Water Resources Agency, 2006).

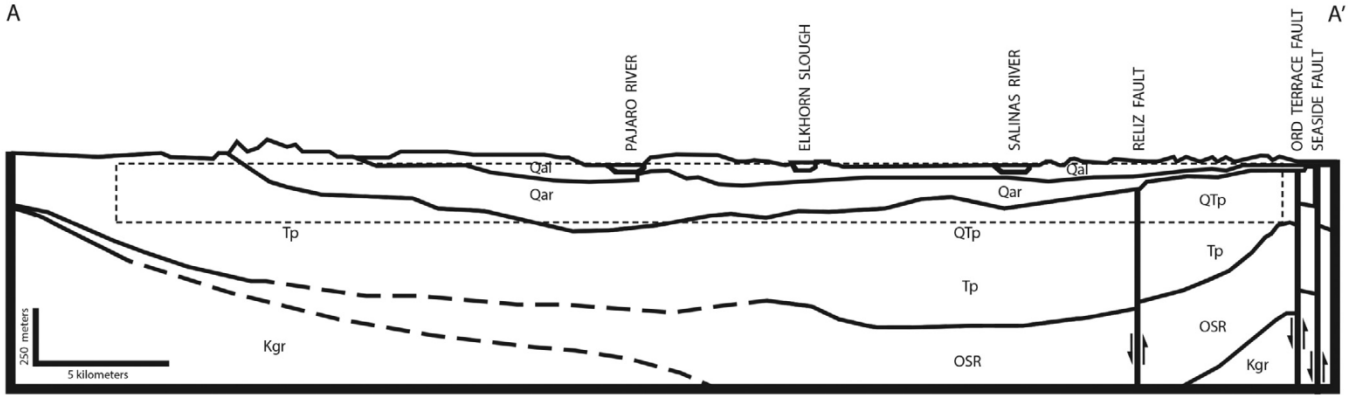

Fig. 2. Conceptual cross-section of geologic formations along the shoreline of Monterey Bay. Developed through compilation of cross-sections from Brabb et al. (1997), Hanson et al. (2002), WRIME (2003), Yates et al. (2005) and Feeney (2007). OSR ('other sedimentary regions') includes the Santa Margarita Formation and Monterey Formation. The dashed box outlines the region spanned by the inverted ERT resistivity profiles.

3. Data Acquisition, Processing, and inversion

In October 2014 long-offset ERT data were collected along 40 km of the Monterey coast. The locations of the ERT transects are shown in black on Fig. 1a. Data were collected on the beach, above the high tide line. The data acquisition line was broken in three locations due to the presence of water bodies or stretches of beach where land access was denied. Electrodes were spaced every 22.5 m, with a total of 81 electrodes along the 1.8 km active cable length. Cable segments were rolled over in 450 m increments to ensure continuous overlap in data acquisition. An ABEM Terrameter system was used to collect data using both a dipole-dipole array and a gradient array to maximize sensitivity to both vertical and horizontal variations in subsurface resistivity (Loke, 2015). This acquisition strategy resulted in 83,875 data points. The data were collected over two weeks by the Geophysics Group from WorleyParsons, based out of Calgary, Canada, along with Stanford University researchers.

Prior to inversion data were excluded based on two criteria: (1) an apparent resistivity of <0.01 Ohm-m or >35 Ohm-m, (2) a recorded standard deviation of >100%, and modeling error >5%. The filtering resulted in a dataset with 67,295 points.

The ERT data were inverted using updated versions of the 2.5D forward modeling and inversion codes described by Pidlisecky and Knight (2008) and Pidlisecky et al. (2007). This code minimizes the objective function in Eq. (1), resulting in an estimated electrical conductivity model that honors the measured data as well as a prior assumption regarding model structure (smoothness),

$$\phi(m) = \frac{1}{2}\|W_d(d(m) - d_{obs}\|^2 + \frac{\beta}{2}(\|\alpha_s W_s(m - m_{ref})\|^2 + \|\alpha_x W_x(m)\|^2 + \|\alpha_z W_z(m)\|^2) \quad (1)$$

where m is the natural log of the EC model, $d(m)$ is the data calculated for a given conductivity model, d_{obs} is the observed data (the measured voltages normalized by the injected current), W_d is a data weighting matrix that contains $\frac{1}{std(d_{obs})+std(d(m))+Pos_{err}+\varepsilon}$ along the diagonal, W_s is a matrix that enforces smallness, W_x and W_z are matrices that enforce flatness in the x- and z-directions respectively, α_s, x, z are parameters that control the weighting of each regularization term, and β is a parameter that controls the overall weighting between regularization and data misfit. W_d was formed using the reported standard deviations for the observations ($std(dobs)$). The modeling error ($std(d(m))$) was estimated by comparing numerical results to analytical solutions for a homogeneous conductivity structure. Positional error (Pos_{err}) is calculated using the expected data error associated with a random positional/projection error of 2.5 m on the electrode positions (e.g., GPS error + projection error). This positional error is particularly important when using mixed-array types, as different arrays have different sensitivity to positional error. Tidal variations can be a possible noise source in coastal ERT studies; however, previous numerical modeling suggested this component would be negligible given the spatial scale of the survey and the relatively small tidal change (1–2 m) (Pidlisecky et al., 2015). The final term, ϵ, in the error matrix serves to penalize small data values and was taken as 1e−5 (Oldenburg and Li, 2005). We assume α_s is 1×10^{-4}, α_x is 5, α_z is 1, and β is calculated based on the size of the dataset. The inversion used a two-stage approach where ε was reduced from 1e−4 to 1e−5. This has a similar effect to decreasing β with the added benefit of increasing the sensitivity to the low amplitude data as the inversion progresses.

The starting models for the inversions were homogeneous models with the electrical resistivity of a saltwater-saturated sediment (0.9 ohm-m). No additional data were used to constrain the inversions. Results gave an absolute mean percent error ranging from 7.9 to 12.4%, after four iterations of the inversion algorithm for each of the ERT sections. While better fits can be achieved with a single array type, the larger error is a worthwhile sacrifice for the improved image detail and depth of investigation gained from combining multiple array types.

The success of the acquisition, processing, and inversion of data at this unique scale for coastal groundwater studies depended on a number of advances in hardware, software, and operational logistics. Specifically: using the multichannel ABEM Terrameter and multi electrode cables allowed for rapid data collection; the roll along method allowed for continuous data profiles far beyond the length of the active array; collection on the beach allowed for excellent coupling between electrodes and the ground; GPS measurements of electrode position allowed for minimization of position-related error; and long offsets between electrodes allowed for deeper imaging. Even with these advances, there were some challenges associated with this type of acquisition: longer offsets in electrodes results in smaller amplitudes of signal at the longest offsets, as well as greater sensitivity to noise; and the presence of low resistivity features (saltwater intrusion) in the near surface impacted the ability to image to depth beneath these features. The challenges associated with the long offsets were address by varying the injected current during acquisition to obtain a signal comparable to that used at smaller offsets. For this survey, the maximum injected current was 0.5 amps. To address the issue of decreased resolution with depth as a result of low resistivity features near the surface, inverted resistivity profiles were clipped at 280 m as that was the maximum depth of interest for this study. A depth of investigation analysis, performed as part of the processing workflow (Oldenburg and Li, 1991), confirmed the repeatability of large-scale features within this zone of interest.

4. Results and discussion

Fig. 3 shows the inverted resistivity profiles from the ERT data, where color represents log10 resistivity values. The figure is shown from the perspective of looking inland from Monterey Bay. These profiles extend down to 280 m.b.s.l., and are hung at sea level with an 5x exaggerated digital elevation model to illustrate the surface topography along the coast. The region spanned by the inverted resistivity section is shown as the dashed box in Fig. 2. The log10 resistivity values range from −0.2 ohm-m, interpreted as saltwater intruded regions, to 2.2 ohm-m interpreted as freshwater regions. It is important to note that while variation in pore fluid salinity will cause variation in subsurface resistivity in regions with saltwater intrusion, changes in lithology, specifically in clay content, can also have an impact on subsurface resistivity. Table 1 shows the expected resistivity values in this region for different lithologies, with different pore fluid salinity. These values were estimated from the Seaside Basin Water Master Sentinel well e-logs at depths where the drilling report identified the fluid type, and where lithologic type (ie sand, clay, or silt) assigned in the driller's lithology log could be corroborated with the gamma log. Ten data points met these criteria and were used to produce the values in Table 1. This table leads us to interpret the lowest resistivities in the inverted resistivity section as corresponding to the presence of saltwater, and the highest resistivities as corresponding to freshwater. Between these two end members, variation in lithology introduces uncertainty in the determination of fluid salinity.

The complex resistivity distributions shown in Fig. 3 suggest complicated patterns of saltwater intrusion that could be difficult to characterize with spatially sparse wells alone. In order to validate the features found in these resistivity sections, and understand what new information could be gained from these exploratory data that could not be inferred from existing data sets

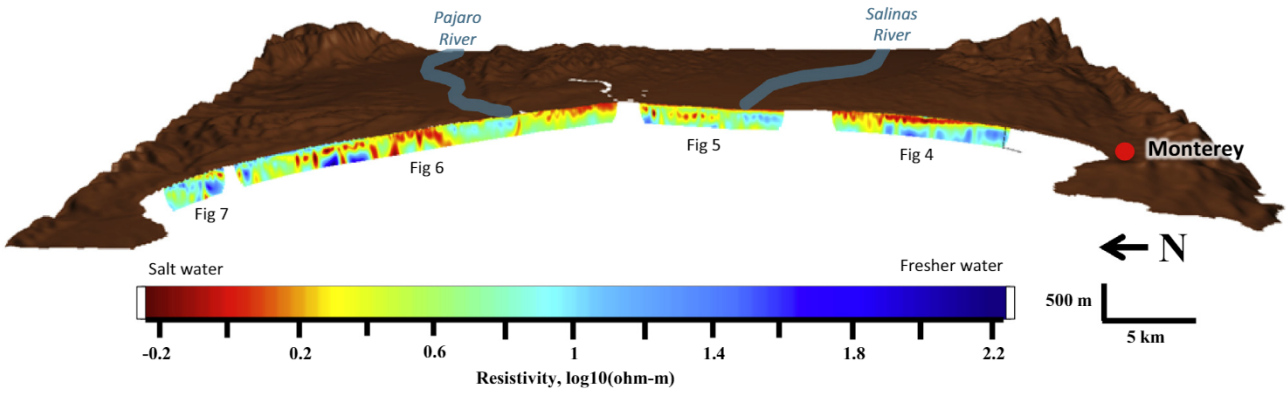

Fig. 3. Inverted electrical resistivity sections along the Monterey Bay coast where color displays log resistivity values. Sections are hung at sea level along a digital elevation model (DEM vertical exaggeration is 5X, data from USGS national elevation dataset). View is from offshore looking towards the coast. Sections are labeled Figs 4–7 corresponding to detailed views of each section to follow.

Table 1
Resistivity (Ohm-m) of select geologic materials, derived from the Seaside Basin Water Master Wells 1–4.

	Sand and Gravel	Silt	Clay
Freshwater Saturated	30–70	No data	7–12
Saltwater Saturated	0.7–3	1.2–3	1.5–5

alone, each profile was compared in great detail with available geologic interpretations and reports, hydrologic reports, land use maps, well logs, and geophysical reports from the region. These comparisons, discussed in detail below, have revealed that ERT data can be useful in identifying where geologic features (such as faults, horizontal clay layers, and paelochannels) are controlling the pattern of intrusion, in identifying where surface water is changing the salinity of underlying sediments, and in identifying where anthropogenic actions (such as pumping from individual wells) is causing saltwater intrusion and controlling the spatial distribution. In many of the comparisons below, it is also shown that ERT data can provide significant new insights that cannot be obtained from the more traditional data sets that are typically available. The detailed interpretations given below are specific to the field site of our study, but serve the important function of demonstrating and validating, with specific examples, the application of this geophysical method as an exploratory tool at and above the basin scale. These examples show the spectrum of features that can be resolved by this method, highlighting the transferability of this approach to other similarly impacted basins around the world. This may be especially important in regions with limited data, where this method could be used to identify specific locations for further data collection, obtain information about spatial heterogeneity in saltwater intruded zones, or to guide setting model boundary conditions. Such uses could greatly improve predictions and management of saltwater intrusion. Furthermore, the detailed interpretations presented below contribute to the limited literature characterizing saltwater intrusion at and above the basin scale in this ecologically and economically significant region in California.

Figs. 4–7 show detailed views of each of the four inverted resistivity sections. Where available, comparable resistivity measurements made in wells have been overlaid on the sections, along with significant boundaries (geologic formations or aquifers) from the geologic cross-sections show in Fig. 1b. These boundaries are shown as solid black lines, except where the original cross-sections denoted uncertainty in the identification or location of the boundaries in which case a dashed black line was used. Where there was no cross-section less than 2.5 km inland, dashed black lines denote interpolation between cross-sections. Formations and/or aquifers are named according to names used in the sources for the cross-section, and are intended for comparison purposes only (rather than implying any interpretation of unit age or depositional environment from the ERT data). This is due to differences in the inferred boundaries in the source materials for the cross-sections. No attempt has been made to force consistency between profiles, as the goal of this interpretation is to compare each individual profile with the local understanding of the subsurface at that location. At present, there does not exist a unified, well-constrained, stratigraphic interpretation that spans the length of our study area. Boundaries unique to the ERT inverted sections have been marked with gray dashed lines. Markers along the bottom of each resistivity section denote key locations referred to in the discussion of the sections.

Fig. 4 shows the southernmost resistivity profile, along the coast of the Seaside Subbasin. The profile is overlain with resistivity measurements taken from coastal monitoring wells, named SBWM 1-4, which were specifically designed for coastal induction resistivity measurements. There is excellent agreement between resistivity measurements made in these coastal monitoring wells, and the inverted ERT resistivity. This was also seen in the pilot study (Pidlisecky et al., 2015). The inverted resistivity profile is fairly consistent with the existing hydrogeologic understanding, but yields new information.

Let us now move from south to north (right to left), looking in detail at the features within this profile. Within this profile low resistivity suggests saltwater intrusion in the upper region (Qal, Qar formations). This is consistent with the current understanding of water quality along this particular stretch of coast, where in wells SBWM1-4 high salinities are inferred, and the water table sits at ~ 20 ft below MSL (Feeney, 2007). In the Feeney (2007) report, a shift from aquifer to clay material is identified at the boundary between the units labeled as Qar and Qtp at wells SBWM3 and SBWM4. Between markers 1 and 2 along the line, we can see the influence of this clay as the saltwater (red in the image) is constrained to the top unit. As we move to the north, there is evidence of the saltwater moving downward into Qtp, suggesting that the clay layer is no longer present. This same observation was made in the pilot study (Pidlisecky et al., 2015). The ERT data do however suggest that there is a flow boundary, such as an aquitard, deeper in the section, preventing the dense higher salinity water in the intruded upper unit from migrating further downward. This boundary is noted with a gray dashed line between markers 2 and 4 and labeled as "vertical flow boundary". The location of

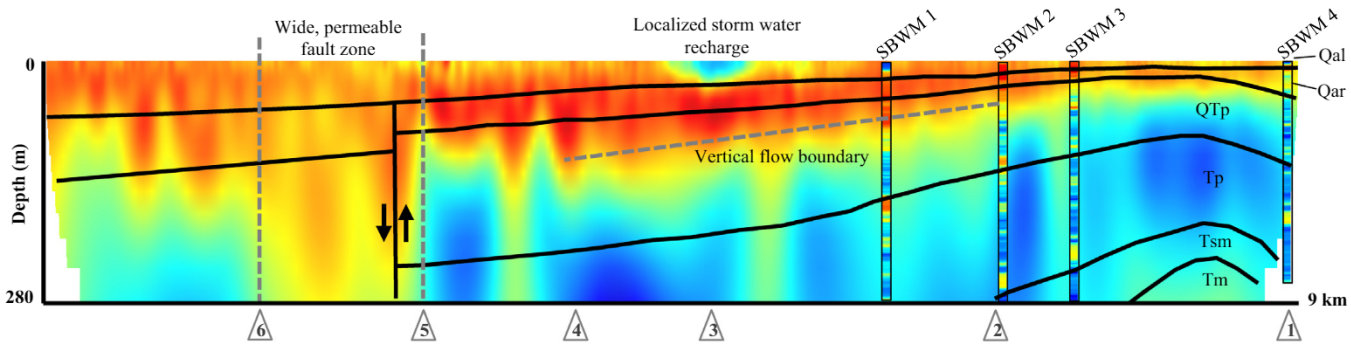

Fig. 4. Inverted ERT resistivity profile overlain with resistivity logs from coastal monitoring wells, formation boundaries from Feeney (2007) geologic cross-section (solid black), and interpretations (dashed gray). Profiles are hung at sea level and extend down 280 m. Markers 1–6 at the bottom of figure point to locations referred to in discussion.

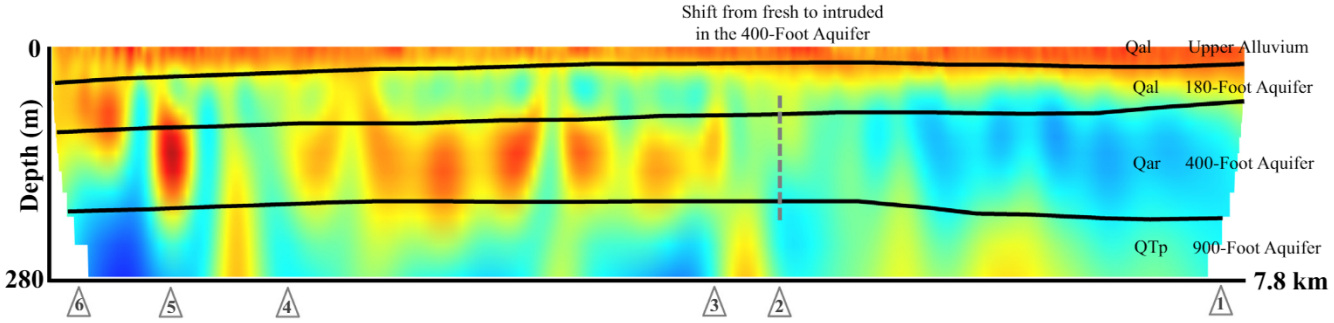

Fig. 5. Inverted ERT resistivity profile overlain with formation boundaries from RBF (2014) geologic cross-section (solid black) and interpretation (dashed gray). Profiles are hung at sea level and extend down 280 m. Markers 1–6 at the bottom of figure point to locations referred to in discussion.

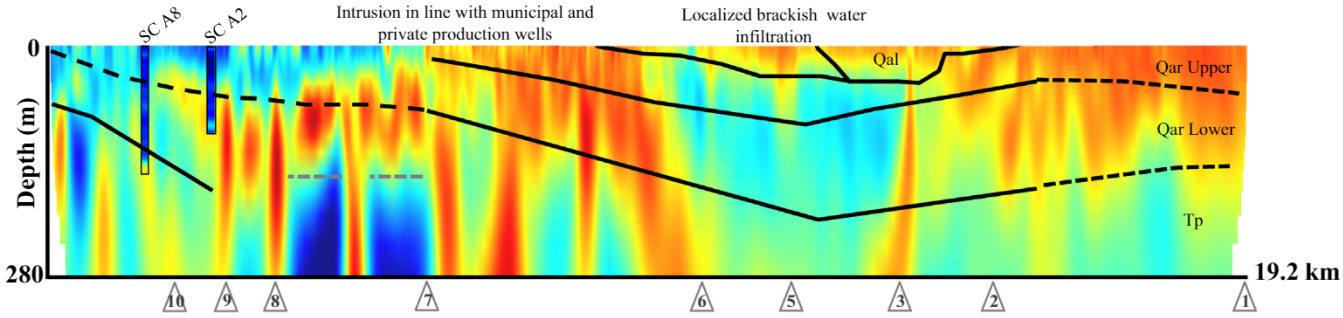

Fig. 6. Inverted ERT resistivity profile overlain with formation boundaries from Hanson et al. (2002) and Brabb et al. (1997) geologic cross-section (solid black), resistivity logs from monitoring wells SC A8 and SC A2, and interpretation (dashed gray). Profiles are hung at sea level and extend down 280 m. Markers 1–10 at the bottom of figure point to locations referred to in discussion.

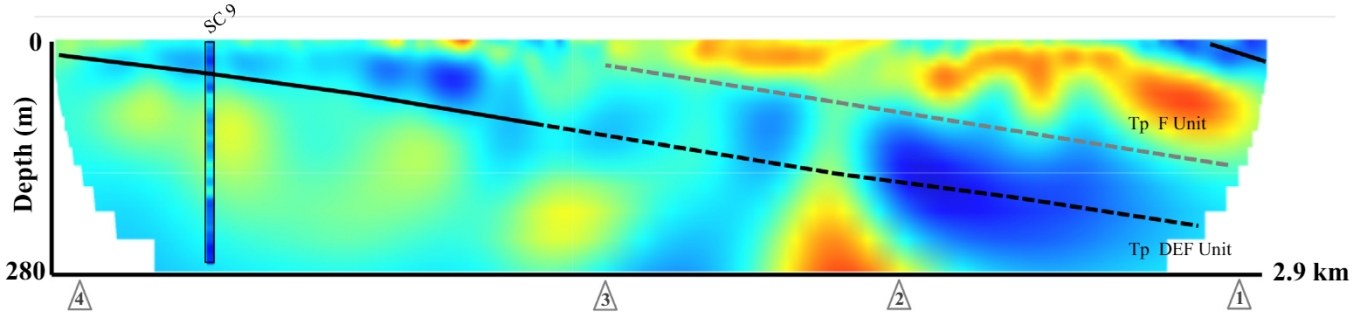

Fig. 7. Inverted ERT resistivity profile overlain with formation boundaries from Brabb et al. (1997) geologic cross-section (solid black), resistivity logs from monitoring wells SC 9 and SC 8, and interpretation (dashed gray). Profiles are hung at sea level and extend down 280 m. Markers 1–4 at the bottom of figure point to locations referred to in discussion.

the boundary coincides with a shift to higher gamma counts (not shown) in SBWM1 and SBWM2, which indicates higher clay content.

Looking deeper, within units Tp and Tsm between markers 1 and 5, the high resistivity values (blue) indicate that these units contain freshwater at the coast. These units are the primary source of groundwater for the city of Seaside, located 2.5 km inland from marker 1.

At marker 3 a high resistivity feature near the surface falls directly beneath diverted storm water ponds, suggesting that the feature is a freshwater lens resulting from storm water infiltration. This feature is significant both because it highlights direct interaction between surface water and the subsurface, and because it shows the ability of ERT to image hydrologic features smaller than would likely be resolved with a monitoring well network.

Between markers 5 and 6, a strong vertical feature in the resistivity profile maps onto the known vertical Reliz Fault. This fault is shown as a single fault in many geologic cross-sections and reports (Feeney, 2007; Hydrometrics, 2009; WRIME, 2003), but is shown to have two splays at the coast in a USGS database showing the surface traces of California faults (USGS and California Geological Survey, 2006). The locations of the faults from this database are shown in red in Fig. 1b. The inverted resistivity section is in agreement with the USGS dataset, the width and sharp boundaries of the vertical low resistivity (orange/red) feature suggesting that there are two splays of a fault at the coast. Furthermore, the boundaries of the low resistivity feature, noted with dashed gray lines at markers 5 and 6, are directly in line with the USGS fault locations at the surface. Here, the ERT clearly reveals that the fault is impacting fluid distribution because of the sharp discontinuity in resistivity at the boundaries of this feature, and the lower resistivity within the fault zone. This resistivity pattern suggests that the fault zone is promoting vertical flow of saltwater from the upper units into the lower ones. Alternately, the fault may be functioning as a barrier to horizontal flow within units below the Qar formation, while increased hydraulic conductivity within the fault zone is enhancing horizontal intrusion from the ocean. Additional data would be needed to determine the exact mechanism(s) through which the fault is impacting flow, as a fault can have a wide variety of influences (Bense and Person, 2006; Jolley et al., 2007).

Fig. 5 shows the resistivity profile along the coast of the 180-Foot/400-Foot Salinas Subbasin. In this profile, while we see strong agreement with the overlain formation boundaries, the inverted resistivity profile also shows significant complexity within the formations. Saltwater intrusion is seen in the Upper Alluvium, across the whole profile, consistent with water sample TDS measurements from wells (RBF, 2014). Between markers 1 and 3 the distribution of the resistivity values suggests that saltwater extends down into the underlying 180-Foot aquifer, while between markers 3 and 6 it remains confined in the Upper Alluvium. This can be explained by the presence of the Salinas Valley Aquitard, a clay layer which emerges at the base of the Upper Alluvium at marker 3, thickens to the north, and reaches a thickness of ~22 m at marker 6 (RBF, 2014). It is the thickness of this clay layer that leads us to conclude that the saltwater in the Upper Alluvium is not hydraulically connected to the low resistivity zone interpreted as salt water within the 180-Foot aquifer at marker 6.

Looking deeper, within the Qar/400-Foot aquifer unit, there is considerable variation in resistivity across the profile. The resistivity values suggest a transition between a region with fresher water to the south and more saline water to the north. This transition, noted with a gray dashed line at marker 2, correlates well with the location of a feature in offshore seismic reflection data collected by the USGS (Dartnell et al., 2016). Dartnell et al. interpreted this feature as a vertical erosional unconformity. The ERT data suggests that this feature impacts groundwater flow, but further information would be needed to confirm this hypothesis.

Between markers 1 and 2, within the Qar/400-Foot aquifer unit, beneath the Salinas River, the large high resistivity (blue) features suggest fresher water within this unit at the coast. This conflicts with high TDS measurements from water samples within this unit just south of the extent of this profile. The most likely explanation for this inconsistency is the presence of channelized saltwater intrusion and freshwater discharge resulting in spatial heterogeneity in salinity that is not captured by water samples in wells. This interpretation is supported by USGS offshore seismic reflection data, which found palaeo-channels in sediments at these depths just offshore of this profile (Dartnell et al., 2016). Other possibilities include the local impacts of pumping near the sampling well, and hydraulic discontinuity between these regions. Given the size of the area with the high resistivity values, we are confident in our interpretation of fresher water in the Qar/400-Foot aquifer unit at this location.

Between markers 2 and 4, the resistivity values within the Qar/400-Foot aquifer suggest saltwater intrusion all along the coast in this area in this aquifer. The shape of the low resistivity features (red in the profile) suggest either saltwater intrusion into channelized sediments or localized regions of intrusion due to nearby pumping wells. Given that saltwater intrusion in this aquifer has been mapped up to 4.8 km inland from these features using salinity measurements made in wells (Monterey County Water Resources Agency, 2014), and the evidence for palaeo-channels from offshore seismic reflection data (Dartnell et al., 2016), we favor the former interpretation. Inland of marker 5, there is less reported saltwater intrusion, so we are unsure whether the feature at marker 5 is a channel carrying saltwater or caused by an unidentified nearby pumping well.

The deepest parts of the resistivity profile, within the QTp / 900-Foot aquifer unit show little evidence of significant saltwater intrusion in the resistivity profile. This is in agreement with the limited investigations into this deep aquifer (WRIME, 2003).

Fig. 6 shows the resistivity profile along the coast of the Pajaro Basin. Note that this profile is significantly longer than any of the other profiles, and thus while there appears to be many more vertical features, much of this is due to the enhanced vertical exaggeration. This profile shows significant evidence of the impact of localized groundwater extraction and surface recharge on the variation in salinity.

At the southern end of the profile, between markers 1 and 2, the low resistivity values indicate saltwater intrusion in the upper and lower Qar. This saltwater could be the result of horizontal or vertical saltwater intrusion, as inland from this feature is both the brackish Elkhorn Slough at the surface, and many agricultural wells with a long history of pumping. Chloride monitoring in wells in this area noted saltwater intrusion beginning in the 1990s.

Moving further north, at marker 3 a vertical low resistivity feature in seen in the profile. The most likely explanation for this feature is the presence of the Watsonville Wastewater ocean outfall pipe, which crosses the ERT profile near the surface where the feature is observed, and then continues offshore. This pipe is larger, shallower, and closer to an electrode than any other known noise source along the profile. Furthermore, there are no known public or private pumping wells at this location that could cause this feature. It has been noted in other studies that near surface conductors, such as this one, can result in noise in ERT inversions (Vickery and Hobbs, 2002).

At marker 5 a low resistivity feature is seen at the surface directly below the Watsonville Slough, suggesting infiltration of brackish surface water down into the subsurface. Again, this highlights the ability of ERT data to identify small-scale features that may be missed by dispersed monitoring well networks.

Between markers 3 and 6, the high resistivity (blue) in Qar Lower suggests fresher water at the coast; this coincides with the location of the Pajaro River (shown in Figs. 1b and 3). Along this stretch of coast, salinity measurements in coastal wells have historically indicated saltwater intrusion. In 2002, in an effort to reduce groundwater extraction, water managers began delivery of recycled water to farms inland of the stretch between markers 2 and 6, covering a total area of ~13 km^2 (Hanson et al., 2014). Since this delivery has begun, coastal monitoring wells have consistently shown decreases in salinity, but with wells (point location information) alone it was unclear the extent of this recovery (Lockwood, 2016). The resistivity data at the coast near these monitoring wells suggest that this recovery in salinity spans the region between markers 2 and 6. In 2009 the program was expanded to include farms inland of the stretch between markers 1 and 2, covering an additional ~19.5 km^2 (Hanson et al., 2014). The ERT resistivity data do not indicate significant recovery in this area, likely because the program has been operating for a shorter time. This interpretation is consistent with well-based monitoring in this region (Lockwood, 2016).

Between markers 6 and 10 are a series of low resistivity features. The features at markers 8, 9, (appearing as vertical red lines) fall in line with active and historically active coastal production wells, all located less than one kilometer inland, and screened in the same geologic unit in which the feature is observed. This suggests that these production wells have caused localized saltwater intrusion. There are many additional low resistivity features between markers 6 and 10 that do not correlate directly with known production wells. We interpret these as strong indications of saltwater intrusion caused by pumping from private wells, many of which are known to be actively pumping along this stretch of coast, but whose locations, screened depths, and pumping rates are not publically available at this time (Lockwood, 2016).

While pumping appears to be the dominant control on the observed resistivity structure along this portion of the profile, geology is likely playing a role in saltwater intrusion north of marker 6. Offshore of this marker, the Qar formation becomes exposed on the seafloor, which could enhance the level of interaction between ocean water and groundwater here. Geology is also likely playing a role in blocking the vertical migration of saltwater in some locations. For example, noted with gray dashed lines between markers 7 and 8 are two locations where there is a sharp transition from low resistivity above to very high resistivity below. Because the dense saltwater (low resistivity) would naturally want to migrate downwards, we conclude that a low permeability layer may be acting as a barrier to flow at these two location. The gap in between these suggests that these may be isolated low permeability layers, or part of a single unit that has been breached (perhaps by a poorly completed well). Additional alternate data would be needed to better understand what is controlling the observed resistivity pattern.

The low resistivity features seen in the lower portion of the Tp formation north of marker 10 match well with decreased resistivity observed in monitoring well SC A8. The agreement is not as good between the resistivity profile and the resistivity log from monitoring SC A2.

Fig. 7 shows the resistivity profile along the coast of the Pajaro Basin in the Soquel Creek region. Note that while this profile appears to have less complexity that the others, this profile, with a length of 2.9 km, is considerably shorter.

At the surface, at marker 1, there is a small area with the high resistivity values indicative of freshwater. The base of this area roughly coincides with the short black line indicating a formation boundary.

Beneath this area, between markers 1 and 3, there is a dipping layer of low resistivity. A number of municipal pumping wells are known to extract from the F unit as close as 2 km inland from the coast (ESA, 2010). We have shown as a dashed gray line the boundary between this layer and the underlying region with resistivity values indicative of the presence of freshwater. However, no reports have been found that describe this boundary. The resistivity values in monitoring well SC 8 show high resistivity, indicative of freshwater, above and below this boundary, in contrast to the low resistivity values seen at the top of the resistivity profile. There are a number of possible explanations for this inconsistency. The most likely explanation is that the induction log collected in SC 8 is not representative of the subsurface. This well is older than all others that were logged, and is part of a nested set of wells in a borehole nearly twice the size of the others. Furthermore, the upper 75 m of the log, where we see disagreement with the ERT resistivity, was sealed with sand cement grout. Invasion of this grout into the permeable Tp F formation could result in anomalously high resistivity values within the well log.

The black solid and dashed formation boundary, taken from the cross-section, runs across the entire profile and in many places appears to be the lower boundary of a dipping layer of fresher water. The presence of freshwater in this area is supported by the high resistivity values observed in monitoring well SC 9. In the lower right corner of the cross-section this lower boundary runs through a large high resistivity feature. This suggests that the dashed portion of the lower cross-section boundary (which is not constrained with any well data at this depth) should be shifted downwards.

Below the black solid and dashed formation boundary, between markers 2 and 4, are resistivity values that suggest a region of moderate salinity, hydraulically separated from the overlying units. This conclusion is supported by the observed decrease in resistivity in monitoring well SC 9 as the well crosses the boundary, as well as existing understandings of this region that identified these two units as separate aquifers based on geologic and hydraulic head data (Hydrometrics, 2014).

5. Conclusions

In this study, we demonstrated the value of spatially continuous information derived from long-offset ERT data, when used in conjunction with traditional data sets, for understanding the distribution of freshwater and saltwater at and above the basin scale, and the geologic and anthropogenic controls on this distribution, along the coast of the Monterey Bay. We used long-offset ERT to obtain electrical resistivity data over an unprecedented distance and depth range for sampling in a region of coastal saltwater intrusion. This was accomplished by utilizing recent advances in acquisition, which allow for more rapid and dense data collection. Within the resistivity profiles we interpreted geological flow conduits and barriers such as palaeo-channels, faults, and impermeable layers; localized saltwater intrusion from nearby pumping wells; infiltration zones of surface fresh and brackish water; and regions where there is significant recovery in water quality, all of which were consistent with existing data and understandings from the region. Complementing traditional data sources (e.g. well logs and head measurements) with ERT data revealed complex spatial patterns of freshwater and saltwater in the subsurface at a level of detail unattainable with the regions traditional mapping and monitoring techniques. While only one case study is presented here, the conclusions regarding the value of this ERT method for continuous exploratory imaging, and the types of features effectively captured in the data, are likely transferable to hydrogeologically similar basins impacted by saltwater intrusion around the world.

A review of the subsurface resistivity images observed in this study also raises the important point, that needs emphasizing as California takes on statewide comprehensive groundwater man-

agement. The influence of geology on the observed distribution of fresh and saltwater strongly supports the management of saltwater intrusion at the scale of relevant geologic boundaries, rather than along political boundaries. This is particularly important in this study area, where there exists a complicated spatial and hierarchical distribution of water management jurisdictions, which tend to follow political, not hydrogeologic, boundaries.

Acknowledgements

This research was initiated with funding from the School of Earth Energy and Environmental Sciences Innovation Fund. Additional funding has been received from the S.D. Bechtel Jr. Foundation, through a gift to the Water in the West program in the Stanford Woods Institute for the Environment, and from the National Sciences and Engineering Research Council of Canada. We are most grateful to Tara Moran who spent over six months managing the complex permitting required to access the beaches of Monterey Bay. We greatly appreciate the assistance we received from: Kevin Fleming, Stephen Bachman, Amy Palkovic, Victor Roth, Tim Hyland, Dan Perry, Chris Spohrer, and Eddie Rhee-Pizano (CA State Parks); Betsey Lynberg and Mary Chavez (Santa Cruz County); Grace Kato (State Lands Commission); Tim Jensen (Monterey Peninsula Regional Parks); Diane Kodama (Salinas River National Wildlife Refuge); Joanna Devers (Big Sur Land Trust); Kim Anderson (Soquel creek Water Management Agency); Brian Lockwood and Casey Meusel (Pajaro Valley Water Management Agency). Thanks to 85 landowners for giving us permission to cross their land, and to the California Coastal Commission for assisting us with the permitting process. The success of this project owes much to the fantastic team from WorleyParsons: Paul Bauman, Laurie Pankratow, Eric Johnson, Keith Brzak, Max Layton; to our field assistants from Stanford: Matias Nordin, Ahmad Behroozmand, Ryan Smith, Dave Cameron; and to Franklin Koch from the University of Calgary. Lastly, we would like to thank two anonymous reviewers whose helpful comments and insights greatly improved this manuscript.

References

Abarca, E., Vázquez-Suñé, E., Carrera, J., Capino, B., Gámez, D., Batlle, F., 2006. Optimal design of measures to correct seawater intrusion. Water Resour. Res. 42. http://dx.doi.org/10.1029/2005WR004524.

Baines, D., Smith, D.G., Froese, D.G., Bauman, P., Nimeck, G., 2002. Electrical resistivity ground imaging (ERGI): a new tool for mapping the lithology and geometry of channel-belts and valley-fills. Sedimentology 49, 441–449. http://dx.doi.org/10.1046/j.1365-3091.2002.00453.x.

Barlow, P.M., Reichard, E.G., 2009. Saltwater intrusion in coastal regions of North America. Hydrogeol. J. 18, 247–260. http://dx.doi.org/10.1007/s10040-009-0514-3.

Batayneh, A.T., 2006. Resistivity tomography as an aid to planning gas-pipeline construction, Risha area, north-east Jordan. Near Surf. Geophys. 4, 313–319. http://dx.doi.org/10.3997/1873-0604.2005053.

Bauman, P., 2005. 2-D resistivity surveying for hydrocarbons–A primer. CSEG Rec. 30, 25–33.

Bear, J., Cheng, A., Sorek, S., Ouazar, D., Herrera, I., 1999. Seawater Intrusion in Coastal Aquifers Theory and Application of Transport in Pourous Media, Illistrate. ed. Springer Science & Business Media, Kluwer, Dordrecht.

Bense, V.F., Person, M.A., 2006. Faults as conduit-barrier systems to fluid flow in siliciclastic sedimentary aquifers. Water Resour. Res. 42. http://dx.doi.org/10.1029/2005WR004480. n/a-n/a..

Brabb, E.E., Graham, S., Wentworth, C., Knifong, D., Graymer, R., Blissenbach, J., 1997. Geologic map of Santa Cruz County, California: a digital database, Open-File Report.

California Water Foundation, 2014. Groundwater Issues Along California's Central Coast.

Carrera, J., Hidalgo, J.J., Slooten, L.J., Vázquez-Suñé, E., 2009. Computational and conceptual issues in the calibration of seawater intrusion models. Hydrogeol. J. 18, 131–145. http://dx.doi.org/10.1007/s10040-009-0524-1.

Dartnell, P., Maier, K.L., Erdey, M.D., Dieter, B.E., Golden, N.E., Johnson, S.Y., Stephen R,H., Cochrane, G.R., Ritchie, A.C., Finlayson, D.P., Kvitek, R.G., Sliter, R.W., Greene, H.G., Davenport, C.W., Endris, C.A., Krigsman, L.M., 2016. California State Waters Map Series—Monterey Canyon and vicinity, California, Open-File Report. doi:http://dx.doi.org/10.3133/OFR20161072.

de Franco, R., Biella, G., Tosi, L., Teatini, P., Lozej, A., Chiozzotto, B., Giada, M., Rizzetto, F., Claude, C., Mayer, A., Bassan, V., Gasparetto-Stori, G., 2009. Monitoring the saltwater intrusion by time lapse electrical resistivity tomography: the Chioggia test site (Venice Lagoon, Italy). J. Appl. Geophys. 69, 117–130. http://dx.doi.org/10.1016/j.jappgeo.2009.08.004.

Department of Water Resources, 2003. California's Groundwater, Bulletin 118 Update 2003.

ESA, 2010. Soquel Creek Water District Well Master Plan.

Feeney, M., 2007. Seaside Groundwater Basin Watermaster Seawater Sentinel Wells Project.

Goldman, M., Kafri, U., 2006. Hydrogeophysical applications in coastal aquifers. In: Appl. Hydrogeophys.. Springer, Netherlands, pp. 233–254.

Hanson, R.T., Everett, R.R., Newhouse, M.W., Crawford, S.M., Pimentel, M.I., Smith, G. A., 2002. Geohydrology of deep-aquifer system monitoring-well site at Marina, Monterey County, California. Water-Resources Investig. Rep.

Hanson, R.T., Schmid, Wolfgang; Faunt, C.C., Lear, Jonathan, Lockwood, B., 2014. Integrated Hydrologic Model of Pajaro Valley, Santa Cruz and Monterey Counties, California: U.S. Geological Survey Scientific Investigations Report 2014–5111. doi: http://dx.doi.org/10.3133/sir20145111.

Hydrometrics, 2009. Basin Management Action Plan Seaside Goundwater Basin, Monterey County California.

Hydrometrics, 2014. Soquel-Aptos Area Groundwater Management Annual Review and Report Water Year 2014.

Johannes, R., 1980. The ecological significance of the submarine discharge of groundwater. Mar. Ecol. Prog. Ser. 3, 365–373. http://dx.doi.org/10.3354/meps003365.

Jolley, S.J., Barr, D., Walsh, J.J., Knipe, R.J., 2007. Structurally complex reservoirs: an introduction. Geol. Soc. London Spec. Publ. 292, 1–24. http://dx.doi.org/10.1144/SP292.1.

Kinzelbach, W., Bauer, P., Siegfried, T., Brunner, P., 2003. Sustainable groundwater management – Problems and scientific tools. Episodes – Newsmag. Int. Union Geol. Sci. 26, 279–284.

Knight, R., Endres, A.L., 2005. An introduction to rock physics principles for near-surface geophysics. In: Near-Surface Geophysics. Society of Exploration Geophysics, Tulsa, pp. 31–70.

Lockwood, B., 2016. Personal Communication.

Loke, M.H., 1999. Electrical imaging surveys for environmental and engineering studies. A practical guide to, 2.

Loke, M.H., 2015. Tutorial : 2-D and 3-D electrical imaging surveys.

Loke, M.H., Chambers, J.E., Rucker, D.F., Kuras, O., Wilkinson, P.B., 2013. Recent developments in the direct-current geoelectrical imaging method. J. Appl. Geophys. 95, 135–156. http://dx.doi.org/10.1016/j.jappgeo.2013.02.017.

Maillet, G.M., Rizzo, E., Revil, A., Vella, C., 2005. High resolution electrical resistivity tomography (ERT) in a transition zone environment: application for detailed internal architecture and infilling processes study of a rhône river paleo-channel. Mar. Geophys. Res. 26, 317–328. http://dx.doi.org/10.1007/s11001-005-3726-5.

Martínez, J., Benavente, J., García-Aróstegui, J.L., Hidalgo, M.C., Rey, J., 2009. Contribution of electrical resistivity tomography to the study of detrital aquifers affected by seawater intrusion–extrusion effects: The river Vélez delta (Vélez-Málaga, southern Spain). Eng. Geol. 108, 161–168. http://dx.doi.org/10.1016/j.enggeo.2009.07.004.

Monterey County Agricultural Commissioner, 2015. Economic Contributions of Monterey County Agriculture.

Monterey County Water Resources Agency, 2006. Monterey County Groundwater Management Plan.

Monterey County Water Resources Agency, 2014. Historic Seawater Intrusion Map.

Ogilvy, R., Meldrum, P.I., Kuras, O., Wilkinson, P.B., Chambers, J.E., Sen, M.A., Pulido-Bosch, A., Gisbert, J., Jorreto, S., Frances, I., Tsourlos, P., 2009. Automated monitoring of coastal aquifers with electrical resistivity tomography. Near Surf. Geophys. 7, 367–3375. http://dx.doi.org/10.3997/1873-0604.2009027.

Oldenburg, D.W., Li, Y., 1991. Estimating depth of investigation in DC resistivity and IP surveys. Geophysics 64 (2). http://dx.doi.org/10.1190/1.1444545.

Oldenburg, D.W., Li, Y., 2005. Inversion Appl. Geophys.: A Tutorial. http://dx.doi.org/10.1190/1.9781560801719.ch5.

Pajaro Valley Water Management Agency, 2016. Maps. URL: http://www.pvwma.dst.ca.us/about-pvwma/maps.php.

Pidlisecky, A., Knight, R., 2008. FW2_5D: A MATLAB 2.5-D electrical resistivity modeling code. Comput. Geosci. 34, 1645–1654. http://dx.doi.org/10.1016/j.cageo.2008.04.001.

Pidlisecky, A., Haber, E., Knight, R., 2007. RESINVM3D: A 3D resistivity inversion package. Geophysics 72, H1–H10. http://dx.doi.org/10.1190/1.2402499.

Pidlisecky, A., Moran, T., Hansen, B., Knight, R., 2015. Electrical resistivity imaging of seawater intrusion into the monterey bay aquifer system. Groundwater. http://dx.doi.org/10.1111/gwat.12351.

Post, V.E.A., von Asmuth, J.R., 2013. Review: Hydraulic head measurements—new technologies, classic pitfalls. Hydrogeol. J. 21, 737–750. http://dx.doi.org/10.1007/s10040-013-0969-0.

RBF, 2014. Monterey Peninsula Water Supply Project Hydrogeologic Investigation Technical Memorandum (TM1) Summary of Results – Exploratory Boreholes.

Rey, J., Martínez, J., Barberá, G.G., García-Aróstegui, J.L., García-Pintado, J., Martínez-Vicente, D., 2013. Geophysical characterization of the complex dynamics of groundwater and seawater exchange in a highly stressed aquifer system linked

to a coastal lagoon (SE Spain). Environ. Earth Sci. 70, 2271–2282. http://dx.doi.org/10.1007/s12665-013-2472-2.

Sanford, W.E., Pope, J.P., 2009. Current challenges using models to forecast seawater intrusion: lessons from the Eastern Shore of Virginia. USA. Hydrogeol. J. 18, 73–93. http://dx.doi.org/10.1007/s10040-009-0513-4.

Taniguchi, M., Burnett, W.C., Cable, J.E., Turner, J.V., 2002. Investigation of submarine groundwater discharge. Hydrol. Process. 16, 2115–2129. http://dx.doi.org/10.1002/hyp.1145.

U.S. Geological Survey and California Geological Survey, 2006. n.d. Quaternary Fault and Fold Database of the United States. URL: http://earthquake.usgs.gov/hazards/qfaults/.

Vickery, A.C., Hobbs, B.A., 2002. The effect of subsurface pipes on apparent-resistivity measurements. Geophys. Prospect. 50, 1–13. http://dx.doi.org/10.1046/j.1365-2478.2002.00295.x.

Werner, A.D., Bakker, M., Post, V.E.A., Vandenbohede, A., Lu, C., Ataie-Ashtiani, B., Simmons, C.T., Barry, D.A., 2013. Seawater intrusion processes, investigation and management: recent advances and future challenges. Adv. Water Resour. 51, 3–26.

WRIME, 2003. Marina Coast Water District Deep Aquifer Investigative Study.

Yates, E.B.G., Feeney, M.B., Rosenberg, L.I., 2005. Seaside groundwater basin: update on water resource conditions.

Zarroca, M., Bach, J., Linares, R., Pellicer, X.M., 2011. Electrical methods (VES and ERT) for identifying, mapping and monitoring different saline domains in a coastal plain region (Alt Empordà, Northern Spain). J. Hydrol. 409, 407–422. http://dx.doi.org/10.1016/j.jhydrol.2011.08.052.